Journal of Geophysical Research: Space Physics

RESEARCH ARTICLE
10.1002/2017JA024925

Ionospheric Conductance Spatial Distribution During Geomagnetic Field Reversals

Bruno S. Zossi[1,2], Ana G. Elias[1,2], and Mariano Fagre[2,3]

[1]INFINOA (CONICET-UNT) and Laboratorio de Fisica de la Atmosfera, Departamento de Fisica, Facultad de Ciencias Exactas y Tecnologia, Universidad Nacional de Tucuman, San Miguel de Tucumán, Argentina, [2]Consejo Nacional de Investigaciones Cientificas y Tecnicas, Buenos Aires, Argentina, [3]Laboratorio de Telecomunicaciones, Departamento de Electricidad, Electrónica y Computación, Facultad de Ciencias Exactas y Tecnología, Universidad Nacional de Tucuman, San Miguel de Tucumán, Argentina

Key Points:
- Ionospheric conductance spatial structure varies with geomagnetic field secular variation
- Ionospheric conductance spatial gradients increase for a weaker geomagnetic field
- For weaker magnetic fields the ionospheric conductivity layer rises to regions of higher electron density

Correspondence to:
A. G. Elias,
aelias@herrera.unt.edu.ar

Citation:
Zossi, B. S., Elias, A. G., & Fagre, M. (2018). Ionospheric conductance spatial distribution during geomagnetic field reversals. *Journal of Geophysical Research: Space Physics*, *123*, 2379–2397. https://doi.org/10.1002/2017JA024925

Received 25 OCT 2017
Accepted 7 MAR 2018
Accepted article online 12 MAR 2018
Published online 26 MAR 2018

Abstract The conductivity of the ionosphere is extremely important in geophysical processes and plays a critical role in magnetosphere-ionosphere-thermosphere coupling. Understanding its nature is essential to understand the physics of ionospheric electrodynamics. Earth's magnetic field, which varies greatly in geological time scales, is among the main variables involved in ionospheric conductivity. The present field can be approximated by a magnetic dipole that accounts for ~80% of the magnetic field at the Earth's surface, plus multipolar components making up the remaining ~20%. During a polarity transition the field magnitude diminishes to about 10% of its normal value at the expense, most likely, of decreasing the dipolar component and becoming mostly multipolar in nature. The effects of geomagnetic field variations on the spatial structure of Hall and Pedersen conductances are analyzed in the present work considering some possible reversal scenarios. The spatial structure of both conductances changes significantly with sharp spatial gradients. The conductivity peak heights also change, moving to upper heights as expected for weaker field configurations.

1. Introduction

Paleomagnetic measurements show that the Earth's magnetic field varies greatly, with the most drastic changes being polarity reversals that take place on average every ~200,000 years. The duration of the transition period leading to a polarity reversal is a few thousand years (~1,000–8,000 years) (Clement, 2004).

At present-day the Earth's magnetic field can be approximated by a geocentric magnetic dipole with its axis tilted about 11° with respect to the Earth rotation axis (Amit & Olson, 2008). This dipole accounts for ~80% of the magnetic field of the Earth's surface, while the remaining ~20% is made up by nondipolar components (Merrill et al., 1998).

Although the understanding of geomagnetic reversals has improved considerably over the years with paleomagnetic studies and geodynamo simulations, its properties, which involve the uncertainty about the dominance of a dipolar or multipolar configuration during a polarity transition, are still under discussion (Jacobs, 1994; Valet et al., 2012; Valet & Fournier, 2016). The main characteristic is that the axial dipole vanishes during a reversal when the dipole axis crosses the equator. Amit et al. (2010) summarized several scenarios for a reversal, of which two extremes for the dipolar component are a dipole collapse and a dipole rotation from one hemisphere to the other. In this last case, only the axial dipole would vanish by transferring its energy to the equatorial components. Regarding the nondipolar field, Amit et al. (2010) consider three main possibilities. It may (1) decrease and recover in phase with the dipole collapse, (2) remain unchanged, or (3) grow throughout the reversal possibly due to energy transfer from the dipole, or dynamo configurations favoring the generation of a nondipolar field.

Glassmeier, Soffel, et al. (2009), using large-scale geodynamo simulations, indicate that multipoles of higher order than the dipole are likely to prevail in the Earth's core field during a polarity transition. In addition, observational evidence for the transition field scenario characterized by a reduced dipole moment and significant to dominant higher-order multipoles was provided by Leonhardt and Fabian (2007) in a study of the Matuyama-Brunhes reversal based on high-quality paleomagnetic records. Leonhardt et al. (2009) contrasted this transition field configuration with results for the Laschamp excursion.

There are many environmental properties that depend on the Earth's magnetic field. One is the flux of high-energy particles entering the Earth's upper and middle atmosphere which is shielded by the geomagnetic

field. During polarity reversals the magnetospheric shielding would be far lower than normal (Glassmeier, Richter, et al., 2009; Olson et al., 2011). The shape and size of the magnetosphere also depends strongly on this field (Glassmeier et al., 2004; Rishbeth, 1985; Siscoe & Chen, 1975; Zieger et al., 2006).

Geomagnetic polarity transition fields with reduced or even zero dipolar contributions and dominant higher-order multipoles have received a lot of attention in the literature already with several works on nondipolar ionospheres and magnetospheres. The first nondipolar contributions are the quadrupole terms of the spherical harmonics expansion of the Earth's magnetic field and have already been addressed by several authors, for example, by Rishbeth (1985) in a study on the quadrupolar ionosphere, Siscoe and Crooker (1976) who investigated the location of auroral zones, Biernat et al. (1985) as well as Leubner and Zollner (1985) presenting analytical magnetospheric models, Vogt and Glassmeier (2000) who studied the topology of the radiation belts and the ring current, and Vogt et al. (2004, 2007) who investigated quadrupolar and mixed dipole-quadrupole paleomagnetospheres using magnetohydrodynamic simulations and analytical models.

Among the ionospheric characteristics affected by secular changes in the geomagnetic field are the peak electron density and the corresponding peak height. Several authors analyzed these effects (Cnossen, 2014; Cnossen & Richmond, 2008; Elias, 2009; Elias & Ortiz de Adler, 2006; Yue et al., 2008) searching for an explanation for observed long-term trends at several worldwide ionospheric stations which did not match the expected trends from the increasing concentration of greenhouse gases (Roble & Dickinson, 1989).

Another feature of the ionosphere sensitive to Earth's magnetic field variations is its conductivity that is important in many geophysical processes, playing a critical role in magnetosphere-ionosphere-thermosphere coupling processes. The importance of conductivity to geophysical processes is noticeable from the number of models that need the ionospheric conductivity as an input (McGranaghan, 2016; Rasmussen et al., 1988). In addition, understanding the nature of ionospheric conductivity is essential in order to understand the physics of ionospheric electrodynamics (Richmond & Thayer, 2000). The equations of Hall and Pedersen conductivities depend on the magnitude of the magnetic field through its influence on the ion and electron gyrofrequencies. Magnetic field variations should therefore strongly affect ionospheric conductivity and conductance.

Some studies obtained the Pedersen and Hall conductances parameterized in terms of the geomagnetic field or the dipole moment (Glassmeier et al., 2004; Richmond, 1995; Takeda, 1996; Zieger et al., 2006). Rishbeth (1985), considering a purely quadrupolar geomagnetic field during a polarity reversal, analyzed the ionospheric conductance value in terms of an increase and also a decrease of the total field intensity but without considering the effects over the spatial pattern. Notice that a quadrupolar field implies not only changes in the field intensity but also significant changes in its spatial distribution.

Cnossen et al. (2011) were the first to analyze the changes in spatial structure due to magnetic field changes using the Coupled Magnetosphere-Ionosphere-Thermosphere model. They considered the Earth's internal magnetic field as a centered dipole and performed two simulations referred as a "strong dipole" of strength 8.00×10^{22} A m^2 (close to the present-day value), and a "weak dipole" set to 6.00×10^{22} A m^2. They assessed the Hall and Pedersen field-line-integrated conductivity patterns averaged over 13–15 UT and averaged over the Northern and Southern Hemispheres. The greatest variations were observed on the dayside, being the Hall conductance ~60%–65% larger for the weak dipole than for the strong dipole and ~50%–60% larger in the case of the Pedersen conductance. In a later work by Cnossen et al. (2012), a larger range of dipole moments was considered together with different solar activity level conditions, showing in this case the global mean conductance. Cnossen and Richmond (2012), with the same model, analyzed the variation of Hall and Pedersen conductances integrated over high magnetic latitudes, due to changes in the dipole tilt angle between 0 and 60°. Their results show that these conductances are larger when the magnetic pole of the hemisphere in question is tilted more toward the Sun.

Three elements are essential for determining ionospheric conductivity: plasma density, geomagnetic field strength, and the frequency at which charged particles collide with other atmospheric constituents. Consequently, there is an important change with daytime and with the solar cycle. In the auroral zone, there is in addition great variability due to auroral ionization by precipitating energetic particles (Richmond & Thayer, 2000).

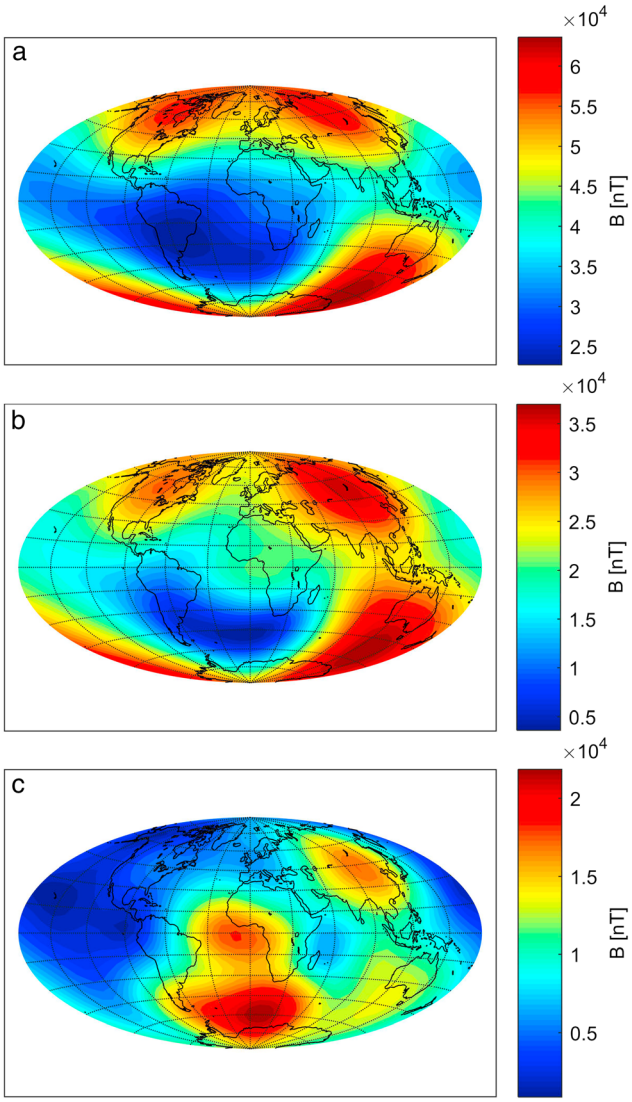

Figure 1. Spatial structure of the intensity of Earth's magnetic field, *B* (nT), obtained from International Geomagnetic Reference Field for 2008 (a) while keeping constant the multipolar field contribution, (b) 50% decrease of dipolar components, and (c) null dipolar components. Note the different scales.

In the present work the spatial structures of Hall and Pedersen conductances are analyzed in terms of geomagnetic field variations, considering first a transition from the present to a nondipolar configuration. The latter consists of a null dipolar component, while maintaining the present multipolar field contribution. Three other end member scenarios for a reversal summarized by Amit et al. (2010) were also considered. The model and procedure used here to obtain conductances, although not as complex as models with magnetohydrodynamic considerations, allows manipulating the Earth's magnetic field in a simple way in order to understand the effects of its secular variation over different characteristics of ionospheric conductivity and conductance. This would be an advantage over most Earth system models which are generally extremely complex due to the complexity of the system itself and act as "black boxes" limiting a deep understanding of the studied process (Nof, 2008; Polvani et al., 2017).

2. Methodology

2.1. Basic Equations

Pedersen and Hall conductances, $\sum_1$ and $\sum_2$, are the height-integrated conductivities given by

$$\sum_1 = \int_{z_1}^{z_2} \sigma_1 \, dz \tag{1}$$

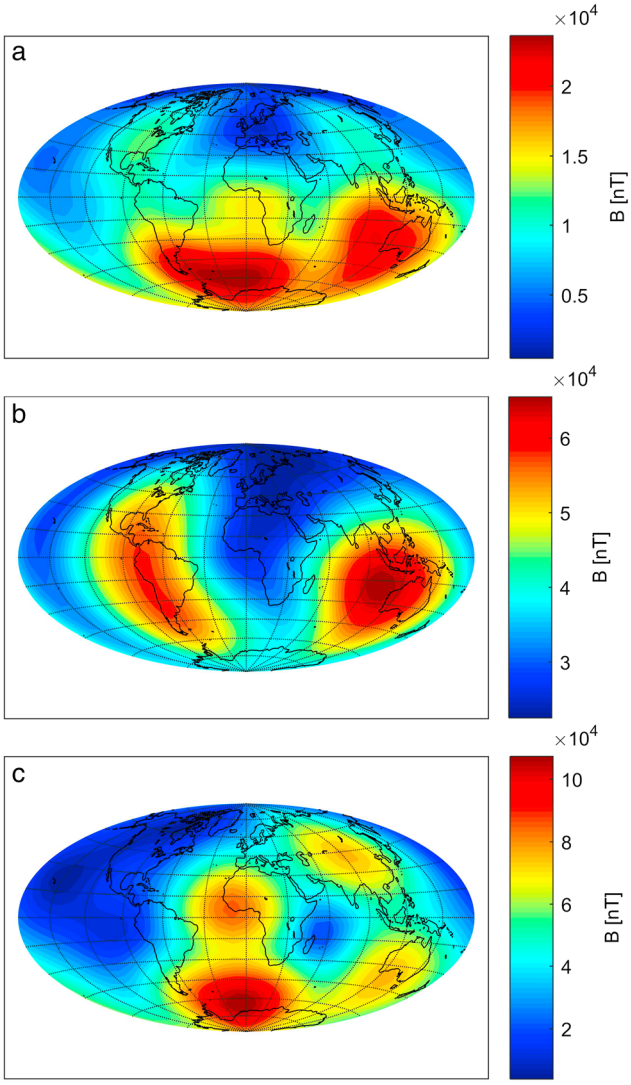

Figure 2. Spatial structure of the intensity of Earth's magnetic field, B (nT), obtained from International Geomagnetic Reference Field for 2008, considering (a) axial dipole collapse, (b) dipole rotation where axial dipole energy is transferred to the equatorial dipole, and (c) energy cascade where dipolar energy is transferred to the quadrupolar and octupolar terms. Note the different scales.

$$\sum\nolimits_2 = \int_{z_1}^{z_2} \sigma_2 \, dz \tag{2}$$

where σ_1 and σ_2 correspond to Hall and Pedersen conductivities, and z_1 and z_2 are the bottom and top of the ionosphere, respectively.

Conductivities are given by Moen and Brekke (1990), Rishbeth and Garriott (1969), and Takeda and Araki (1985)

$$\sigma_1 = N_e e^2 \left[\frac{1}{m_e} \cdot \frac{\nu_e}{(\nu_{e^2} + \omega_{e^2})} + \sum\nolimits_i \frac{f_i}{m_i} \cdot \frac{\nu_i}{(\nu_{i^2} + \omega_{i^2})} \right] \tag{3}$$

$$\sigma_2 = N_e e^2 \left[\frac{1}{m_e} \cdot \frac{\omega_e}{(\nu_{e^2} + \omega_{e^2})} - \sum\nolimits_i \frac{f_i}{m_i} \cdot \frac{\omega_i}{(\nu_{i^2} + \omega_{i^2})} \right] \tag{4}$$

where subscripts e and i stand for electron and ions, respectively, N_e is the electron density, m the mass, e the electron charge, ν the collision frequency, $\omega = eB/m$ the gyrofrequency, B the Earth's magnetic field intensity, and f the relative density of each ion species. Plasma neutrality and single positive charged ion species are assumed.

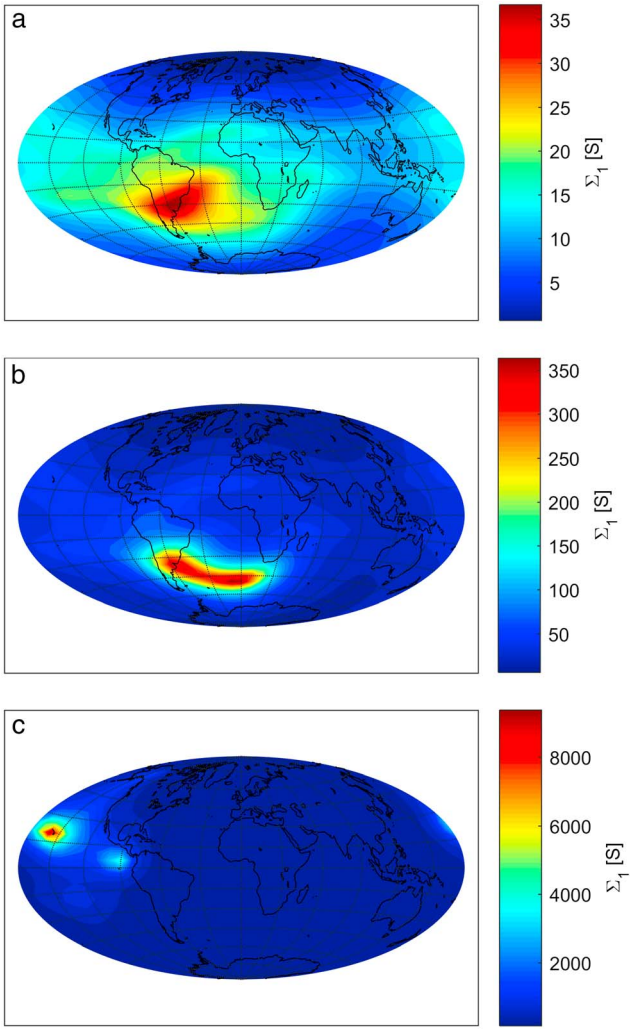

Figure 3. Pedersen ionospheric conductance, $\sum_1$ (S), considering Earth's magnetic field obtained from International Geomagnetic Reference Field for 2008 (a) while keeping constant the multipolar field contribution, (b) 50% decrease of dipolar components, and (c) null dipolar components. Electron density and neutral parameters were kept constant for 3 January (quiet day) and 12 LT conditions. Note the different scales.

Collision frequencies of electrons and ions are given by

$$\nu_e = \nu_{en} + \nu_{ei} \tag{5}$$

$$\nu_i = \nu_{in} + \nu_{ie} \tag{6}$$

where ν_{en} and ν_{ei} are the electron-neutral and electron-ion collision frequencies, respectively, and the same applies to ion collision frequencies. In the ionosphere at heights where the conductivity is significant $\nu_{en} \gg \nu_{ei}$ and $\nu_{in} \gg \nu_{ie}$, so $\nu_e = \nu_{en}$ and $\nu_i = \nu_{in}$ is in general assumed. Taking into account the decrease in Earth's magnetic field here analyzed, and the consequent lift of the conducting layer, $\nu_i = \nu_{in}$, is still valid but not in the case of electrons. So we considered $\nu_e = \nu_{en} + \nu_{ei}$ but still assumed $\nu_i = \nu_{in}$.

Collision frequencies, in s^{-1}, for each type of collision, were calculated from the equations used by the Thermosphere-Ionosphere Electrodynamic General Circulation Model (High Altitude Observatory, 2017; Schunk & Nagy, 2009).

To clarify why the conductivity depends on the magnetic field, we provide below a brief explanation. In any conducting medium, for example, a metallic conductor or plasma as it is the case of the ionosphere the

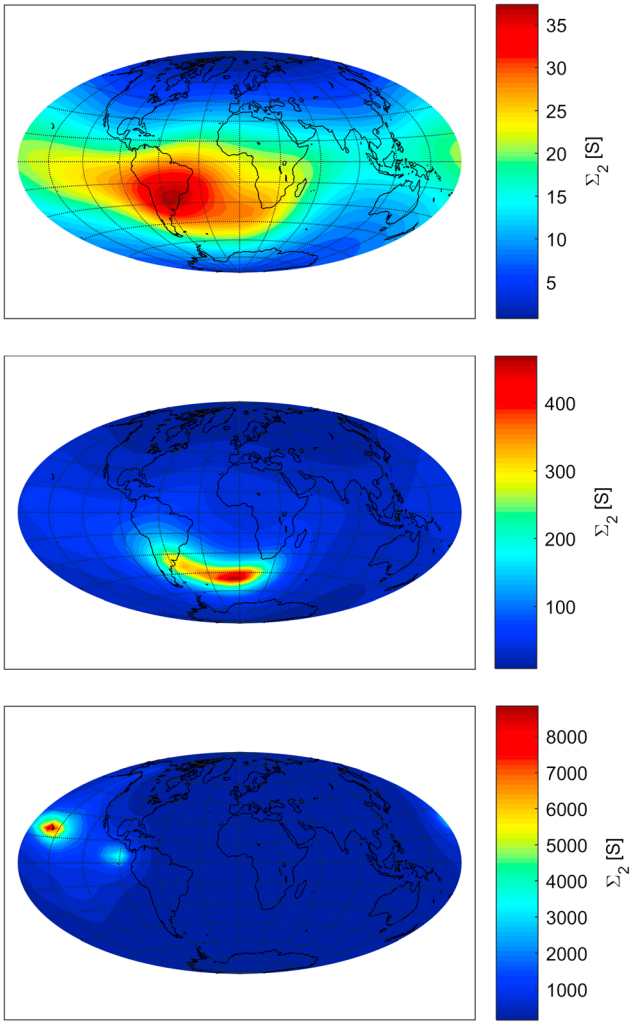

Figure 4. As in Figure 3 for Hall conductance.

conductivity σ is a tensor which relates an electric current density J to an applied electric field E through the Ohm's law.

$$J = \sigma E \tag{7}$$

In the absence of a magnetic field, for spatially isotropic media, this tensor is diagonal with elements that are all equal and whose nature is determined at the microscopic level of the system. The presence of a magnetic field makes the conductivity an anisotropic quantity even for an isotropic material. Equation (7) becomes in this case

$$J = \sigma(E + V \times B) = \sigma E' \tag{8}$$

known as the generalized Ohm's law, where in the case of the ionosphere V is the neutrals' velocity at which charged particles are dragged, and E' is the effective electric field.

Considering E with components (E_x, E_y, and E_z) and B along the z direction and adding ions' and electrons' equation of motions in the ionosphere (see, e.g., Rishbeth & Garriott, 1969; Schunk & Nagy, 2009), equation (8) can be written as

$$J = \begin{pmatrix} \sigma_1 & -\sigma_2 & 0 \\ \sigma_2 & \sigma_1 & 0 \\ 0 & 0 & \sigma_o \end{pmatrix} \begin{pmatrix} E_x - V_{ny}B \\ E_x + V_{ny}B \\ E_z \end{pmatrix} = \sigma_1 E'_{\perp} + \sigma_2 \frac{B \times E'}{B} + \sigma_o E_z \tag{9}$$

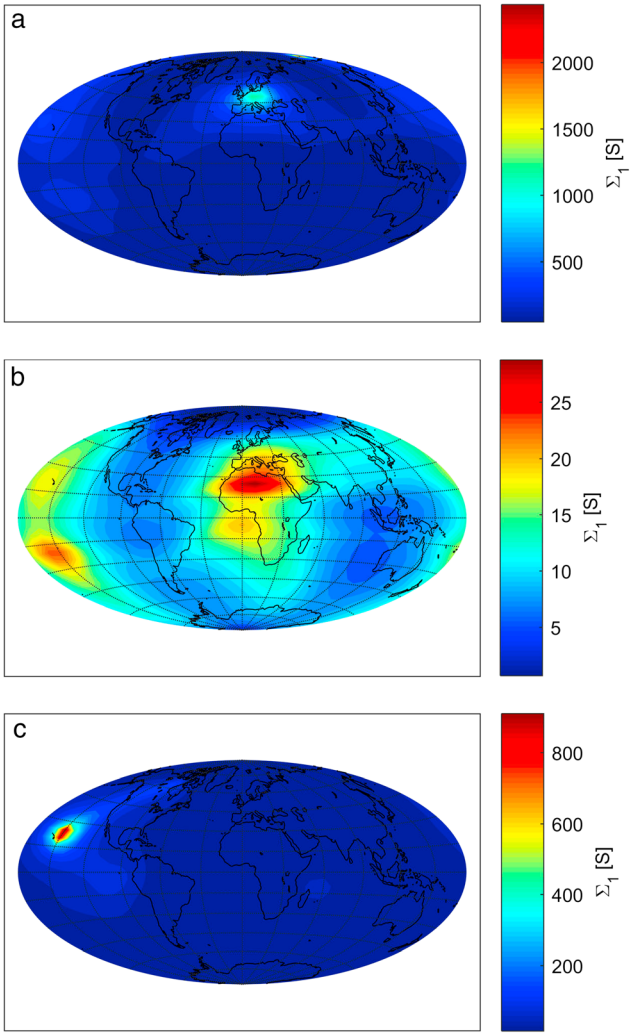

Figure 5. Pedersen ionospheric conductance, $\sum_1$ (S), considering Earth's magnetic field obtained from International Geomagnetic Reference Field for 2008, considering (a) axial dipole collapse (note conductance peak ~2500S at ~75°N, ~170°E), (b) dipole rotation, and (c) energy cascade. Electron density and neutral parameters were kept constant for January 3 (quiet day) and 12 LT conditions. Note the different scales.

where σ_1 and σ_2 are the Pedersen and Hall conductivities, respectively, given by equations (3) and (4), oriented perpendicular to the background magnetic field. σ_o is called the parallel conductivity oriented along the magnetic field line and corresponds to the classical conductivity in the absence of magnetic field. $E'_\perp$ is the component of E' perpendicular to B, and E_z is the component of E along B. Note from equation (9) that the total conductivity is actually a tensor.

2.2. Calculation Setup

The spatial structure of Pedersen and Hall conductances was assessed on a grid with 5° latitude and 10° longitude resolution, for 12 LT, during a quiet solstice day (3 January) of a solar minimum epoch (year 2008), for different Earth's magnetic field conditions described in section 2.3.

Equations (1) and (2) were numerically integrated using the trapezoid rule with a simple computer model, that is,

$$\int_{z_1}^{z_2} \sigma dz = \sum \frac{\sigma(z_{i-1}) + \sigma(z_i)}{2} \Delta z \tag{10}$$

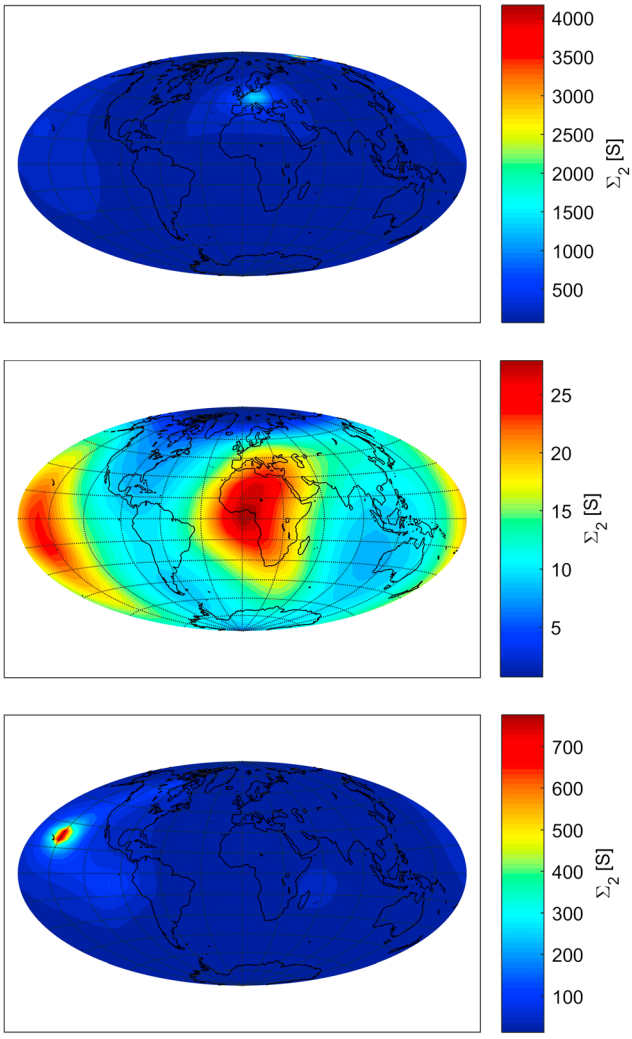

Figure 6. As in Figure 5 but for Hall conductance (In (a) note conductance peak ~4,200 S at ~75°N, ~170°E).

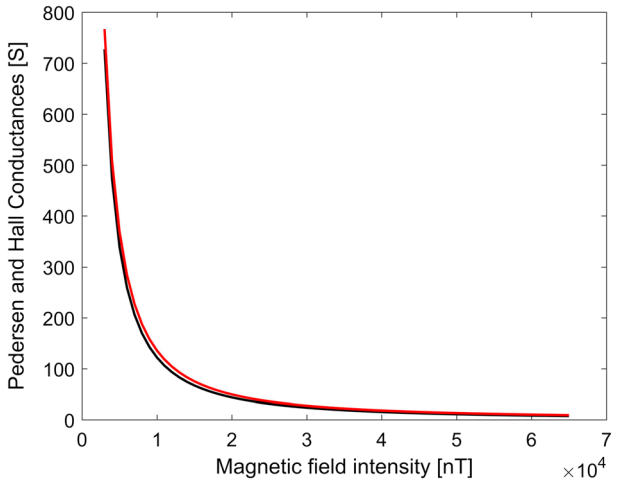

Figure 7. Pedersen (black) and Hall (red) conductances, $\sum_1$ and $\sum_2$ (S), as functions of B (nT), calculated for 20°N, 160°W, for a 3,000–65,000 nT field intensity range.

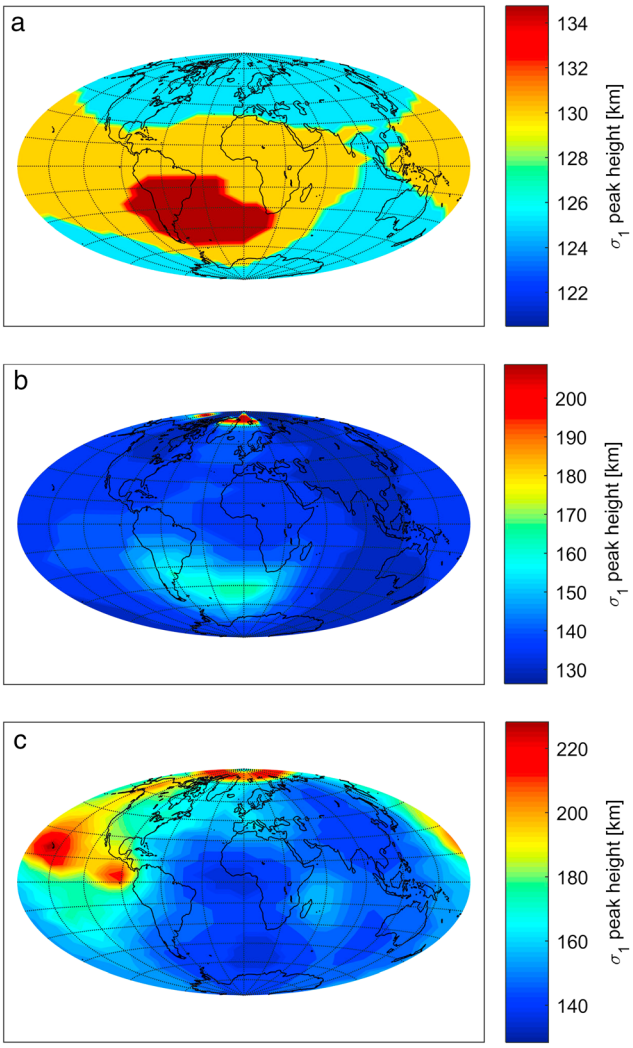

Figure 8. Height of maximum Perdersen conductivity (km) considering Earth's magnetic field obtained from International Geomagnetic Reference Field for 2008 (a) while keeping constant the multipolar field contribution for (b) 50% decrease of dipolar components and for (c) null dipolar components. Electron density and neutral parameters were kept constant for 3 January (quiet day) and 12 LT conditions. Note the different scales.

where z_1 and z_2 were set to 80 and 400 km, respectively, and Δz to 5 km (smaller height steps do not change significantly our results).

The ion species considered for conductivities assessment are the three most abundant at the height range 80–400 km, that is, nitric oxide (NO^+), atomic oxygen (O^+), and molecular oxygen (O_2^+). Ions and electrons were assumed to collide with O_2, O, and N_2 that are the most abundant neutral components at the heights here involved. The parameters needed to assess the different collision frequencies are the temperatures of electrons and ions, T_e and T_i, the neutral concentrations of O_2, O, and N_2, that is N_{O2}, $N_{O,}$ and N_{N2}, respectively, and N_e. T_e, T_i, N_e, and f_i for each ion species were obtained from the International Reference Ionosphere, IRI-2012, (Bilitza et al., 2014), and N_O, N_{N2}, and N_{O2} from the NRLMSISE-00 empirical atmospheric model (Picone et al., 2002).

Auroral ionization will not be considered although at high-latitude conductivities are often dominated by this ionization source, especially at night (Richmond, 2011).

2.3. Earth's Magnetic Field Configurations

The International Geomagnetic Reference Field, IGRF (version 12), model was used to specify the magnetic field for present conditions (Thebault et al., 2015). The decreased configurations were obtained from the

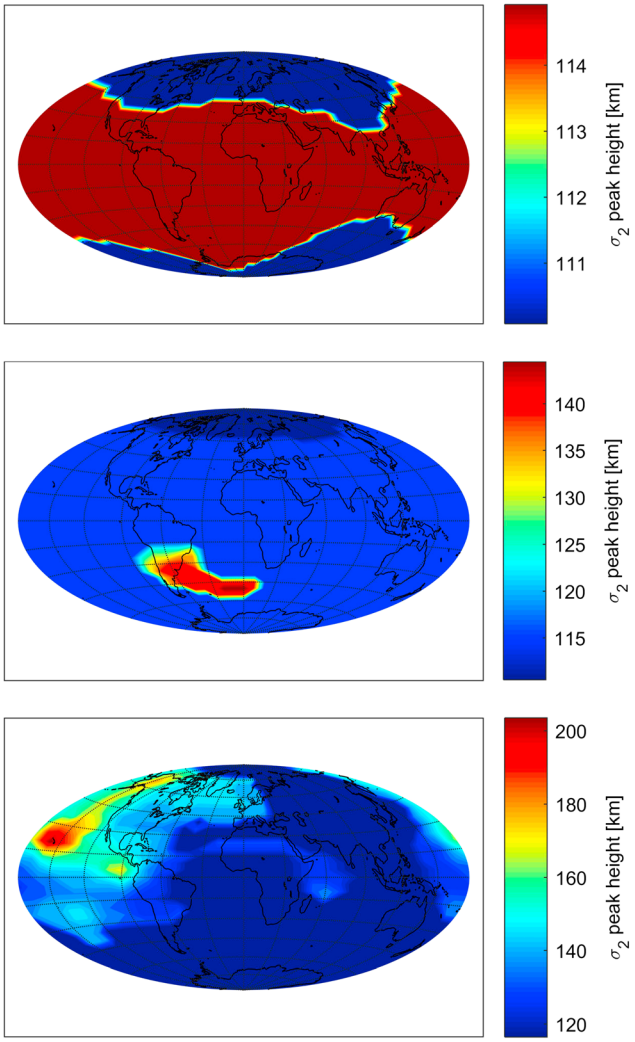

Figure 9. As in Figure 8 for the height of maximum Hall conductivity.

same model modifying the dipolar intensity in the following way. IGRF calculates the geomagnetic field B in terms of the magnetic scalar potential V by $B = -\nabla V$, which is approximated by the series

$$V(r,\theta,\varphi,t) = a\sum_{n=1}^{13}\sum_{m=0}^{n}\left(\frac{a}{r}\right)^{n+1}\left\{\left[g_n^m(t)\cos(m\varphi)+h_n^m(t)\sin(m\varphi)\right]P_n^m(\cos\theta)\right\} \quad (11)$$

where a = 6,371.2 km is the Earth's mean reference spherical radius, r the radial distance from the center of the Earth, θ the geocentric colatitude, φ the east longitude, ${P_n}^m(\cos\theta)$ the Schimdt quasi-normalized associated Legendre functions of degree n and order m, and ${g_n}^m$ and ${h_n}^m$ the Gauss coefficients which are functions of time t. The field was modified first by gradually decreasing the coefficients of the dipolar component, that is, those corresponding to n = 1 (${g_1}^0$, ${g_1}^1$, and ${h_1}^1$) keeping unchanged the higher-order multipolar coefficients.

Figure 1 shows three field instances: the current situation, an intermediate stage where the dipole component was decreased by 50% of its current value, and the final stage consisting of a purely multipolar configuration, that is, ${g_1}^0$, ${g_1}^1$, and ${h_1}^1$ set to zero.

Three other end member scenarios for the reversal summarized by Amit et al. (2010) were also considered: an axial dipole collapse where the axial dipolar component is set to zero while maintaining the equatorial components constant (i.e., only setting ${g_1}^0 = 0$), a dipole rotation where the energy of the axial component is transferred to the equatorial components proportional to their original energies (i.e., setting ${g_1}^0 = 0$ and

increasing g_1^1 and h_1^1), and a third scenario consisting of an energy cascade where the energy of the dipolar components is transferred to the quadrupolar and octupolar components also proportional to the original energy of each degree and order (i.e., setting g_1^0, g_1^1, and h_1^1 to zero and increasing the next 12 Gauss coefficients which correspond to the five quadrupolar and the seven octupolar terms).

Figure 2 shows these three field intensity spatial variations. Note that the dipole rotation scenario (Figure 2b) is incompatible with a decrease of up to ~10% in the geomagnetic field intensity during a reversal (Leonhardt & Fabian, 2007). In contrast, in some numerical dynamo models the equatorial dipole increases during a reversal, suggestive of some contribution of dipole rotation (Olson et al., 2009). In the third reversal scenario it is also possible that the dipole energy is distributed to all multipolar components. However, as the degree increases, the energy decreases significantly with respect to that of lower degrees since the energy is proportional to the square of the degree.

In case of a simultaneous collapse of all degrees and orders of the geomagnetic field, the ionosphere, assuming it will remain, would be isotropic with a scalar conductivity independent of the magnetic field.

3. Results

3.1. Spatial Variability of the Conductances and Height of Maximum Conductivity

The spatial variations of $\sum_1$ and $\sum_2$ are depicted in Figures 3 and 4 for the field configurations shown in Figure 1, and in Figures 5 and 6 for the configurations shown in Figure 2. Except for the dipole rotation scenario (Figure 2b), a clear increase in magnitude is observed in all the other cases, especially over the regions of weakest magnetic field, as expected from the conductivity dependence on B, which is further illustrated in Figure 7. Here as an example, $\sum_1$ and $\sum_2$ are depicted in terms of B varying from 3,000 nT to 65,000 nT for a given location. An emergence of small scales in Figures 3 and 4 that implies an increase in the spatial gradient in those areas is also observed. This is a direct consequence of the "hyperbolic" dependence of $\sum$ on B, clearly seen in Figure 7, which means a steeper increase in $\sum$ for weaker values of B.

Note that there is a qualitative agreement between the patterns of the two conductances, considering the gradual decrease in the dipolar component (Figure 1), with peaks going from South America (full field) to South of Africa (50% of the dipolar component) to north equatorial Pacific (no dipolar component).

In the dipole rotation scenario (Figure 2b) the absence of increased conductances is because the magnetic field at the Earth surface is nowhere weaker than the minimum value of the present field (note the scales in Figures 1a and 2b). This is due to at regions where at present the resulting vector of the dipolar and multipolar field components results in lower values, for this particular reversal scenario, it results in equal or higher ones.

We turn now to the conductivities' height profile. The peak height of σ_1 occurs at the level where $\nu_i = eB/m_i$, which with the present field configuration occurs at ~120 km. σ_2 reaches a maximum in the E region that is ~110 km, since its peak value is more closely related to the peak of the electron density profile. The height of maximum conductivity in the ionosphere then is more sensitive to changes in B for Pedersen than for Hall conductivity. Figures 8 and 9 show the height of maximum conductivity level for the different magnetic fields of Figure 1. A clear uplift of the conducting layer can be noticed in σ_1 as expected from a decrease in B. The conducting layer moves then to heights of greater electron density, eventually reaching the F2 peak (height of greatest electron density in the ionosphere), which also acts to increase the conductivity value. In the case of σ_2 an uplift is also noticed but lower than in σ_1 due to; as already mentioned, σ_2 peak value depends more on the height of maximum electron density.

Figures 10 and 11 show the height of maximum conductivity level for the different reversal scenarios of Figure 2. Here again in the case of the increased equatorial dipole we have a particular situation, that is, an uplift of the conducting layer at the North Pole, due to a weaker magnetic field than the present one in the corresponding region plus the nighttime effect, which is explained in section 5.

3.2. Main Conducting Ions

The dominant ions in the lower ionosphere, particularly in the E region where the conductivity is greater, are NO^+, O_2^+, and O^+, with NO^+ being the most abundant between ~100 km and ~150 km. During the actual

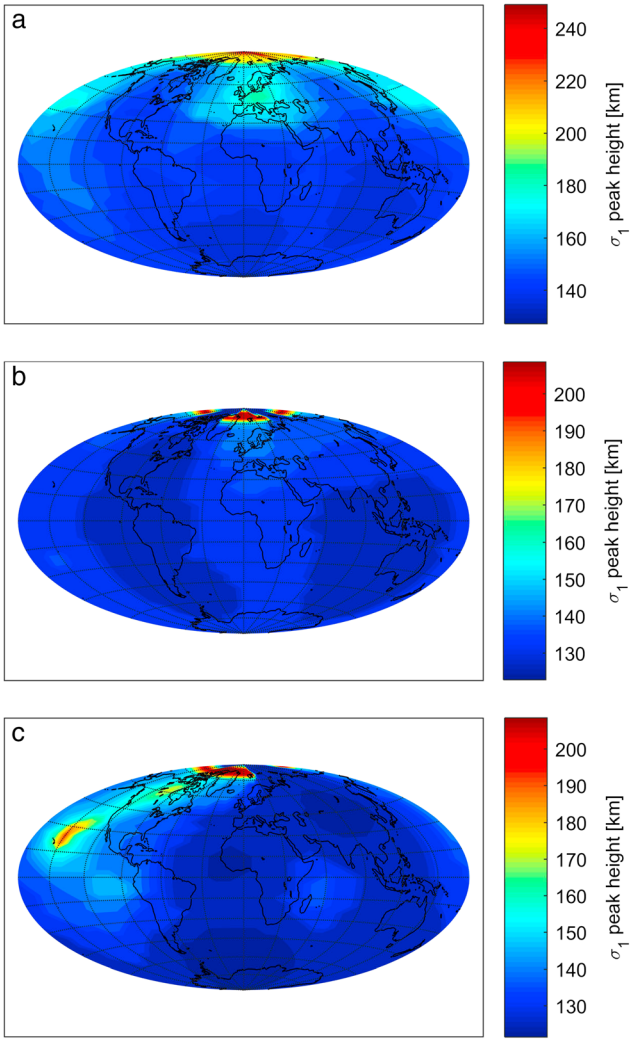

Figure 10. Height of maximum Perdersen conductivity (km) considering Earth's magnetic field obtained from International Geomagnetic Reference Field for 2008, considering (a) axial dipole collapse, (b) dipole rotation, and (c) energy cascade. Electron density and neutral parameters were kept constant for 3 January (quiet day) and 12 LT conditions. Note the different scales.

magnetic field configuration, when the peak height of σ_1 and σ_2 occurs within this height range, the main conducting ion is then NO^+.

However, for a decreased field configuration, the conductivity reaches a maximum at higher levels, and in small regions, it can reach 200 km, and higher, where ~80% of the ions are O^+. As an example, Figure 12 shows the height profile of the different contributions to σ_1 (electrons and each of the three ions considered) for a point where the magnetic field decreases from ~33,000 nT to ~500 nT when the dipolar component is set to zero and where the Pedersen conductivity peaks at ~220 km where the main contribution to σ_1 comes from atomic oxygen ions.

At locations where conductivity are maximal at heights lower than ~200 km, which happens at most of the globe, the conductivities' profile remain similar, with NO^+ being the main conducting ion as it is the case of the present field. Such is the case at 20°S, 50°W, that is the present-day location of the South Atlantic Anomaly, (Aubert, 2015; Finlay et al., 2010; Terra-Nova et al., 2017) where the conductance peaks with the full field (Figures 3a and 4a). However, the peak conductances drift away from this point (Figures 3 and 4) when the dipole intensity decreases and the field intensity minimum drifts (Figure 1). In our other reversal scenarios

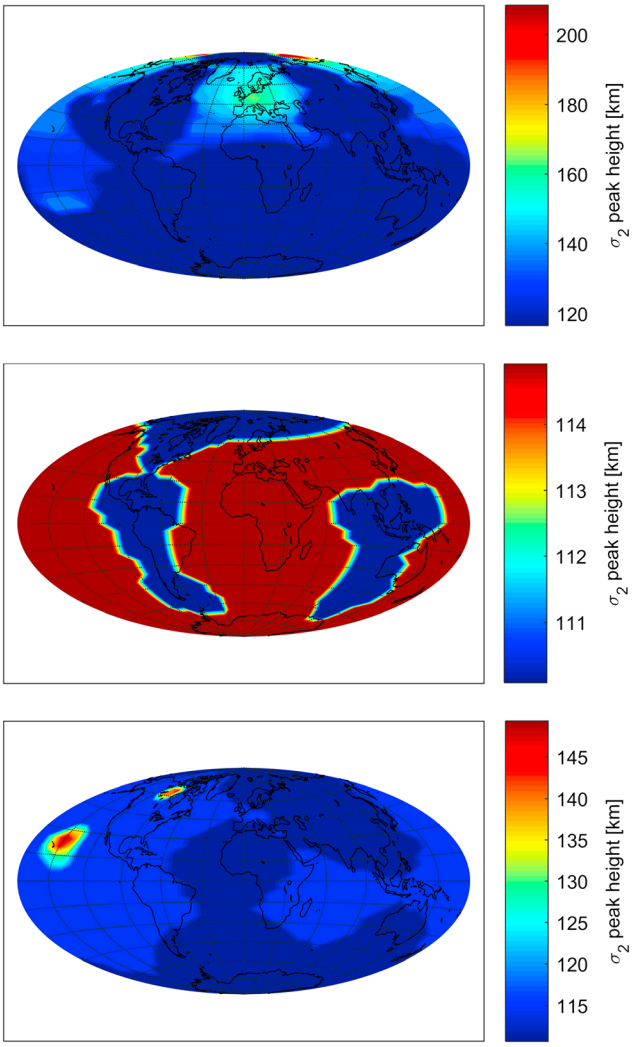

Figure 11. As in Figure 10 for the height of maximum Hall conductivity.

(Figure 2) the peak conductances appear in Europe (Figures 5a and 6a) for axial dipole collapse (Figure 2a), Africa (Figures 5b and 6b) for dipole rotation (Figure 2b), and north equatorial Pacific (Figures 5c and 6c) for energy cascade (Figure 2c).

4. Scaling Relations

In general, scaling relations provide links between variables and are assumed to take a simple power law form. In paleomagnetism, scaling relations were derived associating magnetospheric and ionospheric characteristics to the Earth's dipolar moment magnitude, *M*, under the hypothesis of "self-similarity," that is no change in the shape of the magnetosphere and ionosphere for different values of *M* (Cnossen et al., 2011, 2012; Glassmeier et al., 2004; Siscoe & Chen, 1975; Vogt & Glassmeier, 2001).

To deduce the scaling relations for ionospheric conductances and in order to obtain self-similar conditions while decreasing the Earth's magnetic field, we assessed again $\sum_1$ and $\sum_2$ but considering now a purely dipolar magnetic field with a centered axis coincident with the Earth rotation axis. That is, we set to zero all Gauss coefficient except that corresponding to the centered dipole aligned with the rotation axis, g_1^0. Figure 13 shows as an example $\sum_1$ for two different purely dipolar magnetic field values.

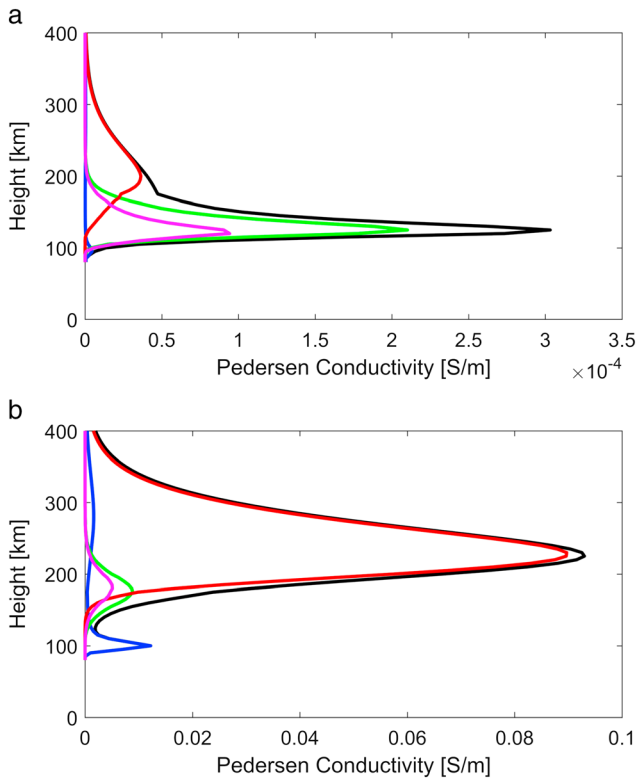

Figure 12. Pedersen conductivity (S/m) profile (black line) at 20°N, 160°W, and conductivities due to electrons (blue line), NO^+ (green), O^+ (red), and O_2^+ (magenta), for 2008 (a) geomagnetic field and (b) only multipolar geomagnetic field.

Figure 14 shows the global averaged $\sum_1$ and $\sum_2$, $\sum_{G1}$, and $\sum_{G2}$, respectively, for 12 LT in terms of M, with scaling relations given by

$$\sum_{G1} \propto M^{-1.45} \tag{12}$$

$$\sum_{G2} \propto M^{-1.40} \tag{13}$$

In a rough analysis the following considerations can be made. For a decrease in the dipolar moment which means a decrease in B, Pedersen conductivity height profile moves to higher altitudes maintaining its shape while Hall conductivity profile maintains the same peak height level but becomes wider. This means that in addition to the expected increase in conductances due to a decrease in B, an additional increase should be added due to N_e increase in the case of Pedersen conductivity (the peak moves closer to the ionosphere F layer peak), and due to an increase in the layer thickness Δh in the case of Hall conductivity, this last reasoning already made by Glassmeier et al. (2004). These effects were estimated obtaining N_e at the corresponding peak heights of σ_1 for decreasing M values together with Δh estimated as $(h_e - h_i)$ where h_e and h_i are the heights with $\nu_e = \omega_e$ and $\nu_i = \omega_i$, respectively. If we assume also scaling relations for the values of N_e at the level of maximum σ_1 and Δh in the case of σ_2, these give $N_e \propto M^{-0.22}$ and $\Delta h \propto M^{-0.27}$. Considering that in addition, both conductivities increase with B^{-1}, this would result in $\sum_{G1} \propto M^{-1.22}$ and $\sum_{G2} \propto M^{-1.27}$. Although these exponents do not coincide with those given in equations (12) and (13) they are a rough approximation.

Relaxing the assumption of self-similarity, we estimated also the scaling relations considering the dipolar and multipolar components of the magnetic field and estimating M as the total magnetic moment:

$$M = \frac{\mu_o}{4\pi} a^3 \left[\sum_{n=1}^{13} (n+1) \sum_{m=0}^{n} \left(g_n^m\right)^2 + \left(h_n^m\right)^2 \right]^{1/2} \tag{14}$$

In this case we obtained $\sum_{G1} \propto M^{-1.59}$ and $\sum_{G2} \propto M^{-1.54}$.

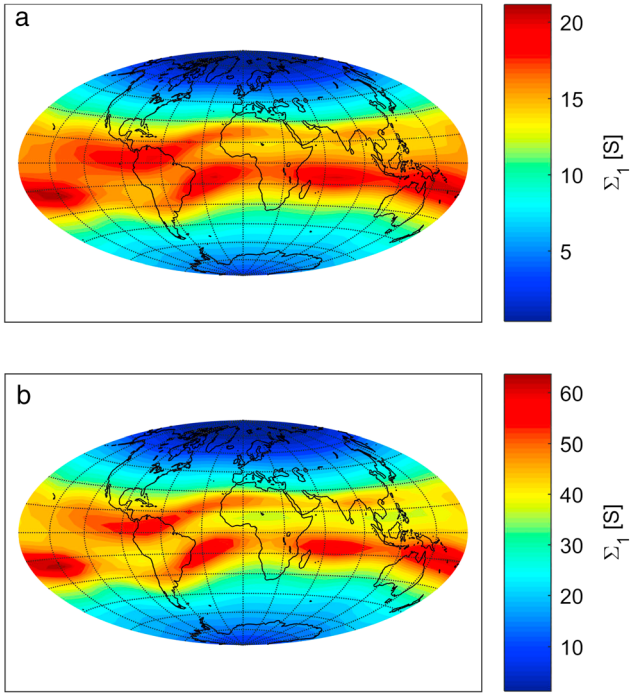

Figure 13. Pedersen ionospheric conductance, $\sum_1$ (S), considering an Earth's magnetic field corresponding to a centered dipole aligned with the rotation axis for International Geomagnetic Reference Field g_1^0 value (a) in 2008 and (b) reduced to 50%.

The exponent values obtained for a dipolar field are similar to those obtained by Cnossen et al. (2012), who for a similar solar activity level obtained $\sum_1 \propto M^{-1.26}$ and $\sum_2 \propto M^{-1.45}$. Glassmeier et al. (2004) obtained $\sum_1 \propto M^{-1}$ and $\sum_2 \propto M^{-1.33}$. They considered a pure dipolar field, a Pedersen conductivity profile shape that does not change significantly but with its peak moving to higher altitudes and a Hall conductivity layer which becomes thicker for weaker fields. The small value of the scaling exponent in the case of $\sum_1$ is due to they consider a Chapman layer with a maximum electron density at 120 km. So when the Pedersen conductivity profile peaks at higher altitudes it encounters lower electron concentrations, which is not the real

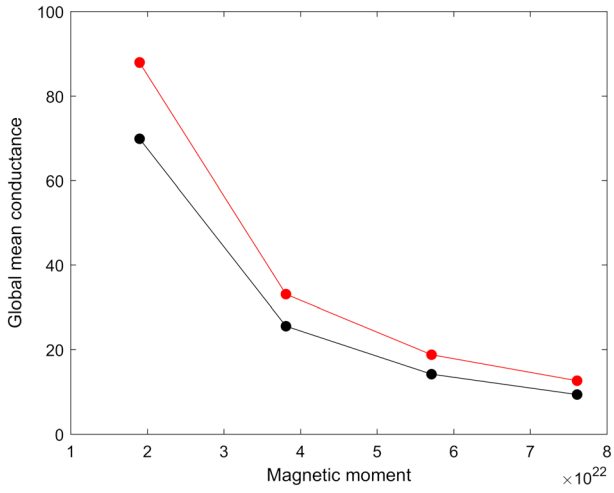

Figure 14. Global averaged Pedersen (black) and Hall (red) conductances (S) for 12 LT as functions of the dipolar moment M (in Am^2) decreasing from its 2008 value to 25%, 50%, and 75%.

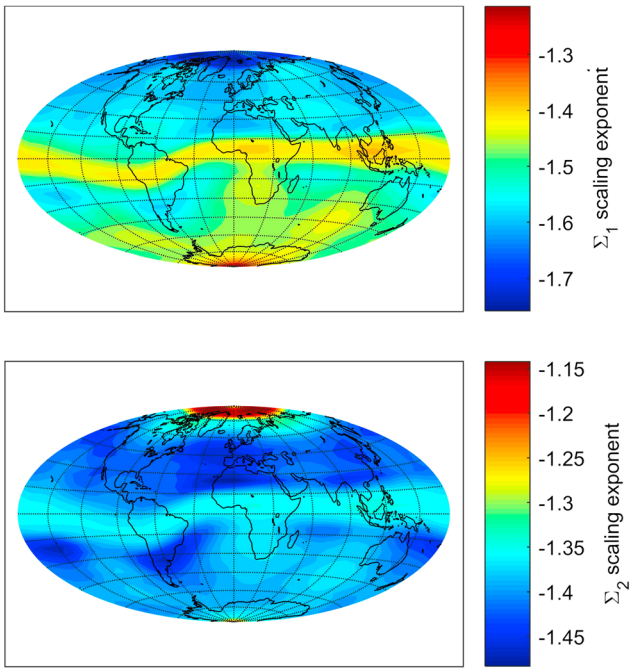

Figure 15. Local scaling exponents obtained as the slope of regressions log($\sum_1$) versus log(M) and log($\sum_2$) versus log(M). Note that conductances vary with location but M remains constant.

situation. Cnossen et al. (2011), with the Coupled Magnetosphere-Ionosphere-Thermosphere model inferred $\sum_1 \propto M^{-1.5}$ and $\sum_2 \propto M^{-1.7}$, which are stronger relations than assumed in previous studies.

We have also estimated "local" scaling exponents, shown in Figure 15, where $\sum_1$ and $\sum_2$ vary with location but M remains constant. The results are practically the same if instead of M we consider the local B. This would not be the case if we consider the magnetic field including multipolar components. The scaling exponents vary almost zonally since the reason for this variation is the variables, other than B, that determine conductances, which present seasonality and other variation patterns which are canceled in the averaging process to obtain global values.

5. Discussion and Conclusions

The spatial structure of the Pedersen and Hall ionospheric conductances changes significantly with geomagnetic field for decreasing dipole moment and different field configurations. Conductivity profiles and the height at which conductivity peaks also change. In addition, an increase is observed in spatial gradients as a consequence of an overall hyperbolic dependence of conductances with B combined with an approach to weaker B values. In the case of dipole rotation where the gradient of the magnetic field at the Earth surface is similar to that of the present field, there is still a significant change in the spatial structure. Note that conductances are maximal at regions close to the magnetic equator where B is weaker, which in this case runs more closely oscillating around a meridian (~10°E).

The spatial gradient variation would directly affect electrojet intensities and field-aligned currents that influence magnetosphere coupling processes. In fact, magnetic field-aligned currents are given by $J_{\parallel}$ = div ($\sum_1 E$) + div ($\sum_2$ (**k** × **E**), where **E** is the electric field vector and **k** the unit vector pointing downward. Here it is clearly seen the dependence on the spatial gradient of Pedersen and Hall conductances (Kelley, 2009). The whole current system in the E layer would be affected not only in magnitude but also in pattern, which would be an extremely interesting estimate to make, of which there is already some backgrounds (Le Sager & Huang, 2002). However, conductances are only one ingredient of the current system. The dynamics of the system and the current strengths in the case of auroral currents are subject to further factors such as magnetospheric size and coupling efficiency which also depend on the Earth's magnetic field.

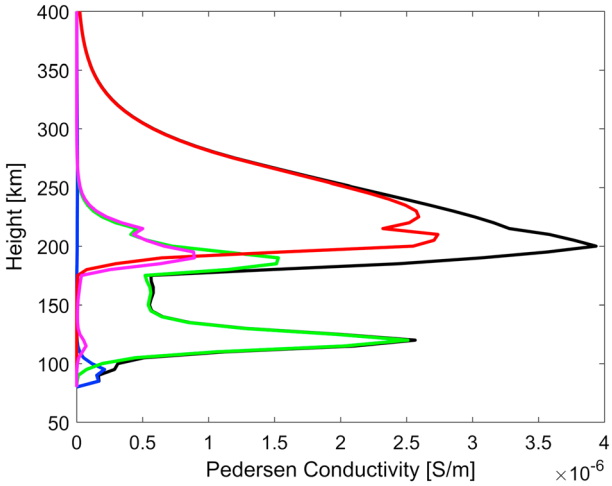

Figure 16. Pedersen conductivity (S/m) profile (black line) at 80°N, 10°W, and conductivities due to electrons (blue line), NO^+ (green), O^+ (red), and $O_2{}^+$ (magenta), for 2008 geomagnetic field with dipolar components decreased by 50%.

It is noteworthy that the peak height of Pedersen conductivity presents the greatest values at ~80°N in the cases shown in Figures 8b and 8c, which correspond to a dipole weaker than the present one, and in the three cases shown in Figure 10. This is because during January, at these high northern latitudes there are 24 h of night. At night, Pedersen conductivity can be maximum in the *F* region, becoming larger than both Pedersen and Hall conductivities of the *E* region (Takeda & Araki, 1985). This effect is enhanced for weaker magnetic fields as can be noticed in Figure 16, which shows σ_1 profile at 80°N, for a geomagnetic field with its dipolar components decreased by 50% (that corresponds to the configuration of Figure 8b). As in Figure 12, Figure 16 shows the different contributions to σ_1 and the total σ_1 in black for which the maximum is clearly at ~200 km that is in the *F* region. Due to the magnetic equator runs almost through the geographic poles in the case of the dipole rotation, the magnetic field results weaker at this location. So even though it is not lower than the weakest field in the present configuration, it is weaker than the present field at the corresponding location.

Something to consider and analyze is that although the formulas for Pedersen and Hall conductivities contain only the magnetic field magnitude, the direction of the local magnetic field vector comes into play through secondary effects such as polarization electric fields. For example, the effective conductivity at the magnetic equator is the Cowling conductivity combining Pedersen and Hall conductivities. So as mentioned previously with regard to the conductances spatial gradient, this would directly affect the current system in the *E* layer.

Another main point related to the direction of the magnetic field is that it is particularly important for coupling processes as it defines the global topology of field lines and thus controls how magnetospheric currents and electric fields can couple to ionospheric dynamics. In the present-day magnetosphere, the strongest interaction is in the auroral zone not only due to the nearly vertical direction of field lines at high latitudes but mostly because remote plasma regions (magnetopause and magnetotail) are connected to the auroral ionosphere in the dipolar magnetic field topology. With higher-order multipoles becoming more important, interactions are expected to be more local.

Acknowledgments
We thank Hagay Amit and an anonymous Reviewer for their constructive and useful comments that have improved this manuscript. We thank ISSI (International Space Science Institute, Bern) and ISSI-BJ (International Space Science Institute, Beijing) for their hospitality and support of the international team on "Climate Change in the Upper Atmosphere" where many ideas in this work were discussed. This work was supported by Projects PIUNT E541 and PICT 2015-0511-Prestamo BID. Data to calculate conductivities and Earth's magnetic field were freely obtained from IRI-2012 (http://omniweb.gsfc.nasa.gov/vitmo/iri2012_vitmo.html), NRLMSISE-00 (http://ccmc.gsfc.nasa.gov/modelweb/models/nrlmsise00.php), and IGRF (http://omniweb.gsfc.nasa.gov/vitmo/igrf_vitmo.html). This work can be replicated using pyglow, a Python package that wraps several upper atmosphere climatological models. The pyglow package is open sourced and available at https://github.com/timduly4/pyglow/. The model and simulations are also available from Bruno S. Zossi upon request (brunozossi@hotmail.com).

References

Amit, H., Leonhardt, R., & Wicht, J. (2010). Polarity reversals from paleomagnetic observations and numerical dynamos simulations. *Space Science Reviews*, *155*(1-4), 293–335. https://doi.org/10.1007/s11214-010-9695-2

Amit, H., & Olson, P. (2008). Geomagnetic dipole tilt changes induced by core flow. *Physics of the Earth and Planetary Interiors*, *166*(3-4), 226–238. https://doi.org/10.1016/j.pepi.2008.01.007

Aubert, J. (2015). Geomagnetic forecasts driven by thermal wind dynamics in Earth's core. *Geophysical Journal International*, *203*(3), 1738–1751. https://doi.org/10.1093/gji/ggv394

Biernat, H. K., Koemle, N. I., & Lichtenegger, H. I. M. (1985). Analytical two-dimensional model of a quadrupole magnetosphere. *Planetary and Space Science*, *33*(1), 45–52. https://doi.org/10.1016/0032-0633(85)90141-2

Bilitza, D., Altadill, D., Zhang, Y., Mertens, C., Truhlik, V., Richards, P., et al. (2014). The International Reference Ionosphere 2012—A model of international collaboration. *Journal of Space Weather and Space Climate*, *4*, A07. https://doi.org/10.1051/swsc/2014004

Clement, B. M. (2004). Dependence of the duration of geomagnetic polarity reversals on site latitude. *Nature*, *428*(6983), 637–640. https://doi.org/10.1038/nature02459

Cnossen, I. (2014). The importance of geomagnetic field changes versus rising CO_2 levels for long-term change in the upper atmosphere. *Journal of Space Weather and Space Climate*, *4*, A18. https://doi.org/10.1051/swsc/2014016

Cnossen, I., & Richmond, A. D. (2008). Modelling the effects of changes in the Earth's magnetic field from 1957 to 1997 on the ionospheric hmF2 and foF2 parameters. *Journal of Atmospheric and Solar-Terrestrial Physics*, *70*(11-12), 1512–1524. https://doi.org/10.1016/j.jastp.2008.05.003

Cnossen, I., & Richmond, A. D. (2012). How changes in the tilt angle of the geomagnetic dipole affect the coupled magnetosphere-ionosphere-thermosphere system. *Journal of Geophysical Research*, *117*, A10317. https://doi.org/10.1029/2012JA018056

Cnossen, I., Richmond, A. D., & Wiltberger, M. (2012). The dependence of the coupled magnetosphere-ionosphere-thermosphere system on the Earth's magnetic dipole moment. *Journal of Geophysical Research*, *117*, A05302. https://doi.org/10.1029/2012JA017555

Cnossen, I., Richmond, A. D., Wiltberger, M., Wang, W., & Schmitt, P. (2011). The response of the coupled magnetosphere-ionosphere-thermosphere system to a 25% reduction in the dipole moment of the Earth's magnetic field. *Journal of Geophysical Research*, *116*, A12304. https://doi.org/10.1029/2011JA017063

Elias, A. G. (2009). Trends in the F2 ionospheric layer due to long-term variations in the Earth's magnetic field. *Journal of Atmospheric and Solar-Terrestrial Physics*, *71*(14-15), 1602–1609. https://doi.org/10.1016/j.jastp.2009.05.014

Elias, A. G., & Ortiz de Adler, N. (2006). Earth magnetic field and geomagnetic activity effects on long term trends in the F2 layer at mid-high latitudes. *Journal of Atmospheric and Solar-Terrestrial Physics*, *68*(17), 1871–1878. https://doi.org/10.1016/j.jastp.2006.02.008

Finlay, C. C., Maus, S., Beggan, C. D., Bondar, T. N., Chambodut, A., Chernova, T. A., et al. (2010). International Geomagnetic Reference Field: The eleventh generation. *Geophysical Journal International*, *183*(3), 1216–1230. https://doi.org/10.1111/j.1365-246X.2010.04804.x

Glassmeier, K. H., Richter, O., Vogt, J., Mobus, P., & Schwalb, A. (2009). The sun, geomagnetic polarity transitions, and possible biospheric effects: Review and illustrating model. *International Journal of Astrobiology*, *8*(3), 147–159. https://doi.org/10.1017/S1473550409990073

Glassmeier, K. H., Soffel, H., & Negendank, J. F. W. (2009). *Geomagnetic field variations*. Berlin: Springer.

Glassmeier, K. H., Vogt, J., Stadelmann, A., & Buchert, S. (2004). Concerning long-term geomagnetic variations and space climatology. *Annales Geophysicae*, *22*(10), 3669–3677. https://doi.org/10.5194/angeo-22-3669-2004

HAO, High Altitude Observatory (2017). TIEGCM V1.94 model description. Boulder, CO: National Center for Atmospheric Research. Retrieved from http://www.hao.ucar.edu/modeling/tgcm/doc/description/model_description.pdf

Jacobs, J. A. (1994). *Reversals of the Earth's magnetic field*. Cambridge, UK: Cambridge University Press. https://doi.org/10.1017/CBO9780511524929

Kelley, M. C. (2009). *The Earth's ionosphere. Plasma physics and electrodynamics* (2nd ed.). CA: Academic Press.

Le Sager, P., & Huang, T. S. (2002). Ionospheric currents and field-aligned currents generated by dynamo action in an asymmetric Earth magnetic field. *Journal of Geophysical Research*, *107*(A2), 1025. https://doi.org/10.1029/2001JA000211

Leonhardt, R., & Fabian, K. (2007). Paleomagnetic reconstruction of the global geomagnetic field evolution during the Matuyama/Brunhes transition: Iterative Bayesian inversion and independent verification. *Earth and Planetary Science Letters*, *253*(1-2), 172–195. https://doi.org/10.1016/j.epsl.2006.10.025

Leonhardt, R., Fabian, K., Winklhofer, M., Ferk, A., Kissel, C., & Laj, C. (2009). Geomagnetic field evolution during the Laschamp excursion. *Earth and Planetary Science Letters*, *278*(1-2), 87–95. https://doi.org/10.1016/j.epsl.2008.11.028

Leubner, M. P., & Zollner, K. (1985). The quadrupole magnetopause. *Journal of Geophysical Research*, *90*(A9), 8265–8268. https://doi.org/10.1029/JA090iA09p08265

McGranaghan, R. M. (2016). Determining global ionospheric conductivity in the satellite and data assimilation age and assessing its influence on the magnetosphere-ionosphere-thermosphere system. Aerospace Engineering Sciences Graduate Theses & Dissertations, 134. Retrirved from http://scholar.colorado.edu/asen_gradetds/134

Merrill, R. T., McElhinny, M. W., & McFadden, P. L. (1998). *The magnetic field of the Earth*. San Diego, CA: Academic Press.

Moen, J., & Brekke, A. (1990). On the importance of ion composition to conductivities in the auroral ionosphere. *Journal of Geophysical Research*, *95*(A7), 10,687–10,693. https://doi.org/10.1029/JA095iA07p10687

Nof, D. (2008). Simple versus complex climate modeling. *Eos Earth & Space Science News*, *89*(52), 544–545. https://doi.org/10.1029/2008EO520006

Olson, P., Driscoll, P., & Amit, H. (2009). Dipole collapse and reversal precursors in a numerical dynamo. *Physics of the Earth and Planetary Interiors*, *173*(1-2), 121–140. https://doi.org/10.1016/j.pepi.2008.11.010

Olson, P. L., Glatzmaier, G. A., & Coe, R. S. (2011). Complex polarity reversals in a geodynamo model. *Earth and Planetary Science Letters*, *304*(1-2), 168–179. https://doi.org/10.1016/j.epsl.2011.01.031

Picone, J. M., Hedin, A. E., Drob, D. P., & Aikin, A. C. (2002). NRLMSISE-00 empirical model of the atmosphere: Statistical comparisons and scientific issues. *Journal of Geophysical Research*, *107*(A12), 1468. https://doi.org/10.1029/2002JA009430

Polvani, L. M., Clement, A. C., Medeiros, B., Benedict, J. J., & Simpson, I. R. (2017). When less is more: Opening the door to simpler climate models. *Eos Earth & Space Science News*, *98*. https://doi.org/10.1029/2017EO079417

Rasmussen, C. E., Schunk, R. W., & Wickwar, V. B. (1988). A photochemical equilibrium model for ionospheric conductivity. *Journal of Geophysical Research*, *93*(A9), 9831–9840. https://doi.org/10.1029/JA093iA09p09831

Richmond, A. D. (1995). Ionospheric electrodynamics. In H. Volland (Ed.), *Handbook of atmospheric electrodynamics* (Vol. 2, pp. 249–290). Boca Raton, FL: CRC Press.

Richmond, A. D. (2011). Electrodynamics of ionosphere-thermosphere coupling. In M. A. Abdu, D. Pancheva, & A. Bhattacharyya (Eds.), *Aeronomy of the Earth's atmosphere and ionosphere*, *IAGA Special Sopron Book Series* (Vol. 2, pp. 191–202). Netherlands: Springer. https://doi.org/10.1007/978-94-007-0326-1

Richmond, A. D., & Thayer, J. P. (2000). Ionospheric electrodynamics: A tutorial. In S. I. Ohtani, et al. (Eds.), *Magnetospheric current systems* (Vol. 118, pp. 131–146). Washington, DC: American Geophysical Union. https://doi.org/10.1029/GM118p0131

Rishbeth, H. (1985). The quadrupole ionosphere. *Annales Geophysicae*, *3*, 293–298.

Rishbeth, H., & Garriott, O. K. (1969). *Introduction to ionospheric physics*. New York: Academic Press.

Roble, R. G., & Dickinson, R. E. (1989). How will changes in carbon dioxide and methane modify the mean structure of the mesosphere and thermosphere? *Geophysical Research Letters*, *16*(12), 1441–1444. https://doi.org/10.1029/GL016i012p01441

Schunk, R. W., & Nagy, A. F. (2009). *Ionospheres: Physics, plasma physics, and chemistry*. New York: Cambridge University Press. https://doi.org/10.1017/CBO9780511635342

Siscoe, G. L., & Chen, C. K. (1975). The paleomagnetosphere. *Journal of Geophysical Research*, *80*(34), 4675–4680. https://doi.org/10.1029/JA080i034p04675

Siscoe, G. L., & Crooker, N. J. (1976). Auroral zones in a quadrupole magnetosphere. *Journal of Geomagnetism and Geoelectricity*, *28*(1), 1–9. https://doi.org/10.5636/jgg.28.1

Takeda, M. (1996). Effects of the strength of the geomagnetic main field on the dynamo action in the ionosphere. *Journal of Geophysical Research*, *101*(A4), 7875–7880. https://doi.org/10.1029/95JA03807

Takeda, M., & Araki, T. (1985). Electric conductivity in the ionosphere and nocturnal ionospheric currents. *Journal of Atmospheric and Terrestrial Physics*, *47*(6), 601–609. https://doi.org/10.1016/0021-9169(85)90043-1

Terra-Nova, F., Amit, H., Hartmann, G. A., Trindade, R. I. F., & Pinheiro, K. J. (2017). Relating the South Atlantic Anomaly and geomagnetic flux patches. *Physics of the Earth and Planetary Interiors*, *266*, 39–53. https://doi.org/10.1016/j.pepi.2017.03.002

Thebault, E., Finlay, C. C., Beggan, C., Alken, P., Aubert, J., Barrois, O., et al. (2015). International Geomagnetic Reference Field: The 12th generation. *Earth, Planets and Space*, *67*(1), 1–19. https://doi.org/10.1186/s40623-015-0228-9

Valet, J. P., & Fournier, A. (2016). Deciphering records of geomagnetic reversals. *Reviews of Geophysics*, *54*, 410–446. https://doi/org/10.1002/2015RG000506

Valet, J. P., Fournier, A., Courtillot, V., & Herrero-Bervera, E. (2012). Dynamical similarity of geomagnetic field reversals. *Nature*, *490*(7418), 89–93. https://doi.org/10.1038/nature11491

Vogt, J., & Glassmeier, K. H. (2000). On the location of trapped particle populations in quadrupole magnetospheres. *Journal of Geophysical Research*, *105*(A6), 13,063–13,071. https://doi.org/10.1029/2000JA900006

Vogt, J., & Glassmeier, K. H. (2001). Modelling the paleomagnetosphere: strategy and first results. *Advances in Space Research*, *28*, 863–868. https://doi.org/10.1016/S0273-1177(01)00504-X

Vogt, J., Zieger, B., Glassmeier, K. H., Stadelmann, A., Kallenrode, M. B., Sinnhuber, M., & Winkler, H. (2007). Energetic particles in the paleomagnetosphere: Reduced dipole configurations and quadrupolar contributions. *Journal of Geophysical Research*, *112*, A06216. https://doi.org/10.1029/2006JA012224

Vogt, J., Zieger, B., Stadelmann, A., Glassmeier, K.-H., Gombosi, T. I., Hansen, K. C., & Ridley, A. J. (2004). MHD simulations of quadrupolar paleomagnetospheres. *Journal of Geophysical Research*, *109*, A12221. https://doi.org/10.1029/2003JA010273

Yue, X., Liu, L., Wan, W., Wei, Y., & Ren, Z. (2008). Modeling the effects of secular variation of geomagnetic field orientation on the ionospheric long term trend over the past century. *Journal of Geophysical Research*, *113*, A10301. https://doi.org/10.1029/2007JA012995

Zieger, B., Vogt, J., & Glassmeier, K. H. (2006). Scaling relations in the paleomagnetosphere derived from MHD simulations. *Journal of Geophysical Research*, *111*, A06203. https://doi.org/10.1029/2005JA011531